J|A|C|S
ARTICLES
Published on Web 06/30/2006

Control of Ambipolar Thin Film Architectures by Co-Self-Assembling Oligo(*p*-phenylenevinylene)s and Perylene Bisimides

Pascal Jonkheijm,[†] Natalie Stutzmann,[‡] Zhijian Chen,[§] Dago M. de Leeuw,[‡] E. W. Meijer,*[,†] Albertus P. H. J. Schenning,*[,†] and Frank Würthner[§]

Contribution from the Laboratory of Macromolecular and Organic Chemistry, Eindhoven University of Technology, P.O. Box 513, 5600 MB Eindhoven, The Netherlands, Philips Research High Tech Campus 4, 5656 AE, Eindhoven, The Netherlands, and Universität Würzburg, Institut für Organische Chemie, Am Hubland, D-97074 Würzburg, Germany

Received March 31, 2006; E-mail: e.w.meijer@tue.nl; a.p.h.j.schenning@tue.nl

Abstract: Control of thin film morphology by self-assembly of, respectively, p-type oligo(*p*-phenylenevinylene)s (OPV)s and n-type perylenebisimides (PBI)s in solution prior to processing, results in film architectures consisting of uniform rodlike domains as shown by atomic force microscopy. Such films from self-assembled molecules show superior charge-carrier mobility in comparison with films processed from molecular dissolved molecules. Moreover, connecting the OPV and PBI building blocks through hydrogen-bonding interactions creates dyad complexes that cofacially stack in apolar solvents. Ambipolar field-effect transistors constructed from these dyad complexes show two independent pathways for charge transport. In strong contrast, processing of OPV and PBI, that are not connected by hydrogen bonds, form charge transfer donor−acceptor complexes that show no mobility in field-effect transistors presumably due to an unfavorable supramolecular organization.

Introduction

The supramolecular organization of organic semiconductors is an important parameter that determines the performance of optoelectronic devices.[1] For instance, for devices such as solar cells, it is necessary to create a nanostructured supramolecular organization that consists of separate pathways for positive and negative charge transport. To generate such pathways several approaches have been applied. For example, based on the intrinsic tendency of two-component materials to phase separate, hole- (p-type) and electron-transporting (n-type) polymers have simply been mixed resulting in phase-separated films on the nanoscale.[2] Yet, phase separation passes several stages of coarsening resulting in different film morphologies.[3,4] Consequently, the preparation method plays an important role in controlling the phase separation and, ultimately, the device performance. Extensive research on phase-segregated blends of, for example, polyfluorene-based polymers show that structural instability of the film architectures results in decreased energy-conversion efficiency.[5,6] In another contribution, the decreased device performance was related to diffusion of organic molecules through the polymer matrix into large crystals thereby increasing the dimension and extent of phase separation.[7,8] Chemical or radiation-induced cross-linking in the solid state[9] or the use of p−n block copolymers[10] have been used to prevent uncontrolled phase separation in the solid state. Improved phase separation has also been reported for liquid-crystalline p-type hexabenzocoronene in combination with a n-type perylene bisimide in which the latter crystallizes yielding a laminated p−n layer.[11]

Our groups have recently constructed self-assembled p-type **OPV$_4$UT**[12,13] fibers in apolar solvents and n-type **PBI-1**[14] supramolecular architectures in the solid state (Scheme 1). To create independent pathways for both charge carriers, we have

[†] Eindhoven University of Technology.
[‡] Philips Research High Tech Campus 4.
[§] Universität Würzburg.

(1) For a recent review, see: Hoeben, F. J. M.; Jonkheijm, P.; Meijer, E. W.; Schenning, A. P. H. J. *Chem. Rev.* **2005**, *105*, 1491−1546.
(2) Yu, G.; Gao, J.; Hummelen, J. C.; Wudl, F.; Heeger, A. J. *Science* **1995**, *270*, 1789−1791.
(3) Utracki, L. A. *Polymer Alloys and Blends: Thermodynamics and Rheology*; Hanser: New York, 1989.
(4) Sperling, L. H. *Introduction to Physical Polymer Science*, 2nd ed.; John Wiley & Sons: New York, 1992.
(5) Arias, A. C.; MacKenzie, J. D.; Stevenson, R.; Halls, J. J. M.; Inbasekaran, M.; Woo, E. P.; Richards, D.; Friend, R. H. *Macromolecules* **2001**, *34*, 6005−6013.
(6) Snaith, H. J.; Arias, A. C.; Morteani, A. C.; Silva, C.; Friend, R. H. *Nano Lett.* **2002**, *2*, 1353−1357.
(7) Schuller, S.; Schilinsky, P.; Hauch, J.; Brabec, C. J. *Appl. Phys. A* **2004**, *79*, 37−42.
(8) Yang, X.; Van Duren, J. K. J.; Janssen, R. A. J.; Michels, M. A. J.; Loos, J. *Macromolecules* **2004**, *37*, 2151−2158.
(9) Mueller, C. D.; Falcou, A.; Reckefuss, N.; Rojahn, M.; Wiederhim, V.; Rudati, P.; Frohne, H.; Nuyken, O.; Becker, H.; Meerholz, K. *Nature* **2003**, *421*, 829−831.
(10) Lee, M.; Cho, B.-K.; Zin, W.-C. *Chem. Rev.* **2001**, *101*, 3869−3892.
(11) Schmidt-Mende, L.; Fechtenkötter, A.; Müllen, K.; Moons, E.; Friend, R. H.; MacKenzie, J. D. *Science* **2001**, *293*, 1119−1122.
(12) (a) Schenning, A. P. H. J.; Jonkheijm, P.; Peeters, E.; Meijer, E. W. *J. Am. Chem. Soc.* **2001**, *123*, 409−416. (b) Jonkheijm, P.; Hoeben, F. J. M.; Kleppinger, R.; Van Herrikhuyzen, J.; Schenning, A. P. H. J.; Meijer, E. W. *J. Am. Chem. Soc.* **2003**, *125*, 15941−15949.
(13) Prins, P.; Senthilkumar, K.; Grozema, F. C.; Jonkheijm, P.; Schenning, A. P. H. J.; Meijer, E. W.; Siebbeles, L. D. A. *J. Phys. Chem. B* **2005**, *109*, 18267−18274.
(14) Debije, M. G.; Chen, Z.; Piris, J.; Neder, R. B.; Watson, M. M.; Müllen, K.; Würthner, F. *J. Mater. Chem.* **2005**, *15*, 1270−1276.

Scheme 1. Molecular Structures of OPV_4UT, PBI-1 and the Hydrogen-Bonded Dyad Complex OPV_4T:Pbi-2, *along with a Schematic Representation Proposed for the Self-assembly Process Creating p-type,* n-type, Alternating or Co-facial p/n Type Structures, Respectively[a]

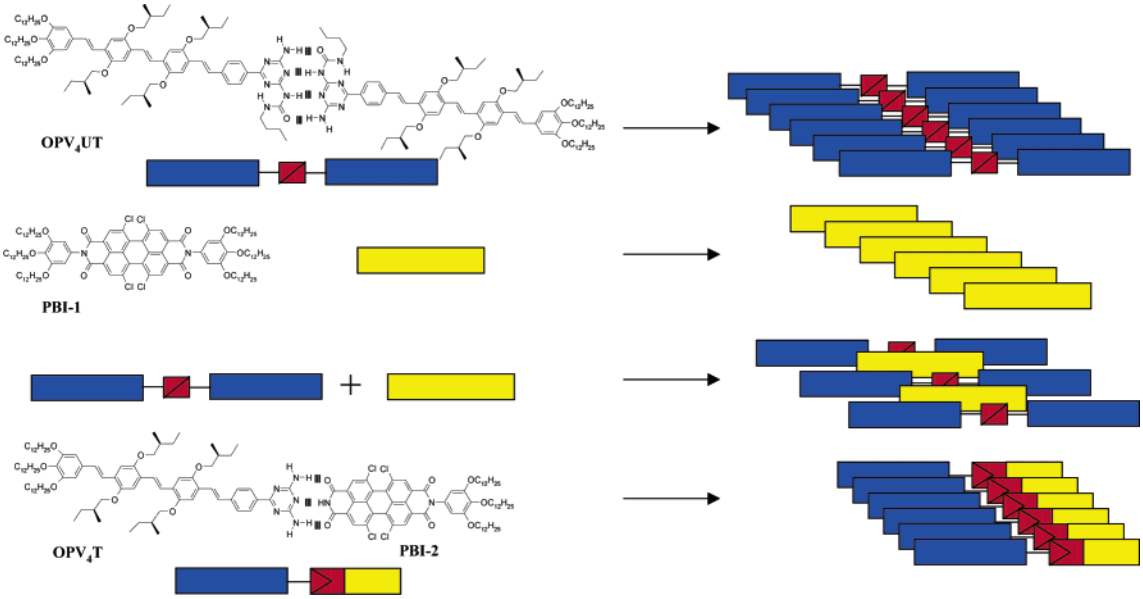

[a] The blue blocks represent the OPV parts, the yellow blocks represent the PB parts and the red shapes represent the hydrogen-bonding units. It should be noted that the angle and distance between the building blocks is of arbitrary choice.

mixed the two individual compounds. Depending on the solvent and the substituents on the perylene bisimide (PBI) and oligo(*p*-phenylenevinylene)s (OPV) derivatives it is found that either mixed aggregates[15] are formed or orthogonally self-assembly takes place yielding separated p- and n-type fibers.[16] In addition, through complementary hydrogen-bonding, we have constructed triad complexes consisting of **OPV_4T** (Chart 1) and a PBI derivative. Bias-dependent scanning tunneling microscopy and cyclic voltammetry measurements have confirmed that such triad complexes consist of electronically disconnected electron donor (OPV) and electron acceptor (PB) units, i.e., a p/n junction.[17] Such triad complexes self-assemble through $\pi-\pi$ interactions in apolar solutions resulting into large supramolecular structures.[18]

Here, we have constructed thin films having a controlled morphology that are processed by spin-coating concentrated solutions containing (i) stacks of either **OPV_4UT** (p-type) or **PBI-1** (n-type), (ii) mixed **OPV_4UT/PBI-1** aggregates, or (iii) the hydrogen-bonded p−n dyad complexes based on **OPV_4T** in combination with an easily accessible **PBI-2**[19] with complementary hydrogen bonds to **OPV_4T**[18] (Scheme 1). We have studied the influence of the solvent on the self-assembly behavior of these species and have characterized the thin-film morphology by atomic force microscopy (AFM). The organization in the films is further probed by measuring charge-transport properties in field-effect transistors. These measurements show in the case of self-assembled single species unipolar charge transport. When p- and n-type building blocks are mixed, ambipolar transport[20] could be measured, but only in cases of an appropriate morphology.

Results and Discussion

Unipolar Assemblies. Self-Assembly in Solution. The self-assembly properties of **OPV_4UT** have been previously re-

(15) Beckers, E. H. A.; Jonkheijm, P.; Schenning, A. P. H. J.; Meskers, S. C. J.; Janssen, R. A. J. *Chem. Phys. Chem.* **2005**, *6*, 2029−2031.
(16) van Herrikhuyzen, J.; Syamakumari, A.; Schenning, A. P. H. J.; Meijer, E. W. *J. Am. Chem. Soc.* **2004**, *126*, 10021−10027.
(17) Miura, A.; Chen, Z.; Uji-i, H.; De Feyter, S.; Zdanowska, M.; Jonkheijm, P.; Schenning, A. P. H. J.; Meijer, E. W.; Würthner, F.; De Schryver, F. C. *J. Am. Chem. Soc.* **2003**, *125*, 14968−14969.
(18) (a) Schenning, A. P. H. J.; van Herrikhuyzen, J.; Jonkheijm, P.; Chen, Z.; Würthner, F.; Meijer, E. W.; Beckers, *J. Am. Chem. Soc.* **2002**, *124*, 10252−10253. (b) Würthner, F.; Chen, Z.; Hoeben, F. J. M.; Osswald, P.; You, C.-C.; Jonkheijm, P.; Herrikhuyzen, J. v.; Schenning, A. P. H. J.; Schoot, P. P. A. M. v. d.; Meijer, E. W.; Beckers, E. H. A.; Meskers, S. C. J.; Janssen, R. A. J. *J. Am. Chem. Soc.* **2004**, *126*, 10611−10618.
(19) The synthesis of **PBI-2** will be published elsewhere: Beckers, E. H. A.; Chen, Z.; Meskers, S. C. J.; Jonkheijm, P.; Schenning, A. P. H. J.; Qing, X.; Osswald, P.; Würthner, F.; Janssen, R. A. J. *J. Phys. Chem. A.*, accepted.
(20) For examples on ambipolar FETs see: (a) Dodabalapur, A.; Katz, H. E.; Torsi, L.; Haddon, R. C. *Science* **1995**, 1560−1562. (b) Tada, K.; Harada, H.; Yoshino, K. *Jpn. J. Appl. Phys.* **1996**, *35*, L944−945. (c) Meijer, E. J.; De Leeuw, D.; Setayesh, S.; van Veenendaal, E.; Huisman, B.-H.; Blom, P. W. M.; Hummelen, J. C.; Scherf, U.; Kadam, J.; Klapwijk, T. M. *Nature Mater.* **2003**, 678−682. (d) Locklin, J.; Shinbo, K.; Onishi, K.; Kaneko, K.; Bao, Z.; Advincula, R. C. *Chem. Mater.* **2003**, 1404−1412. (e) Chesterfield, R. J.; Newman, C. R.; Pappenfus, T. M.; Ewbank, P. C.; Haukaas, M. H.; Mann, K. R.; Miller, L. L.; Frisbie, C. D. *Adv. Mater.* **2003**, 1278−1282. (f) Anthopoulos, T. D.; Tanase, C.; Setayesh, S.; Meijer, E. J.; Hummelen, J. C.; Blom, P. W. M.; De Leeuw, D. *Adv. Funct. Mater.* **2004**, *16*, 2174−2179. (g) Rost, C.; Karg, S.; Riess, W.; Loi, M. A.; Murgia, M.; Muccini, M. *Appl. Phys. Lett.* **2004**, 1613−1615. (h) Babel, A.; Wind, J. D.; Jenekhe, S. A. *Adv. Func. Mater.* **2004**, *14*, 891−898. (i) Tuladhar, S. M.; Poplavskyy, D.; Choulis, S. A.; Durrant, J. R.; Bradley, D. D. C.; Nelson, J. *Adv. Func. Mater.* **2005**, *15*, 1171−1182. (j) Hayashi, Y.; Kanamori, H.; Yamada, I.; Takasu, A.; Takagi, S.; Kaneko, K. *Appl. Phys. Lett.* **2005**, *86*, 052104-1−052104-3. (k) Singh, Th. B.; Gunes, S.; Marjanovic, N.; Sariciftci, N. S.; Menon, R. *J. Appl. Phys.* **2005**, *97*, 114508/1−114508/5.
(21) Würthner, F.; Thalacker, C.; Diele, S.; Tschierske, C. *Chem. Eur. J.* **2001**, *7*, 2245−2253.
(22) Fluorescence lifetime measurements reveal that the decay times of the emission at $\lambda_{em} = 570$ and 650 nm for films spun from heptane (chloroform) are $\tau = 0.30$ ns ($\tau = 65$ ns) and $\tau = 1.1$ ns ($\tau = 1.7$ ns), respectively (see Supporting Information). These differences indicate that the excitations reach trap sites earlier when heptane is used showing that the molecules are more in close contact. Similar observations has been found earlier for self-assembled oligo(*p*-phenylenevinylene) in solution, see: Herz, L. M.; Daniel, C.; Silva, C.; Hoeben, F. J. M.; Schenning, A. P. H. J.; Meijer, E. W.; Friend, R. H.; Phillips, R. T. *Phys. Rev. B.* **2003**, *68*, 045203/1-/7.
(23) Geens, W.; Tsamouras, D.; Poortmans, J.; Hadziioannou, G. *Synth. Met.* **2001**, *122*, 191−192.
(24) Beckers, E. H. A.; Meskers, S. C. J.; Schenning, A. P. H. J.; Chen, Z.; Würthner, F. Janssen, R. A. J. *J. Am. Chem. Soc.* **2006**, *128*, 649−657.
(25) Chen, Z.; Debije, M. G.; Debaerdemaeker, T.; Osswald, P.; Würthner, F. *ChemPhysChem.* **2004**, *5*, 137−140.
(26) Graaf, H.; Michaelis, W.; Schnurpfeil, G.; Jaeger, N.; Schlettwein, D. *Org. Electronics* **2004**, *5*, 237−249.
(27) Sadrai, M.; Bird, G. R.; Potenza, J. A.; Schugar, H. J. *Acta Cryst.* **1990**, *C46*, 637−640.

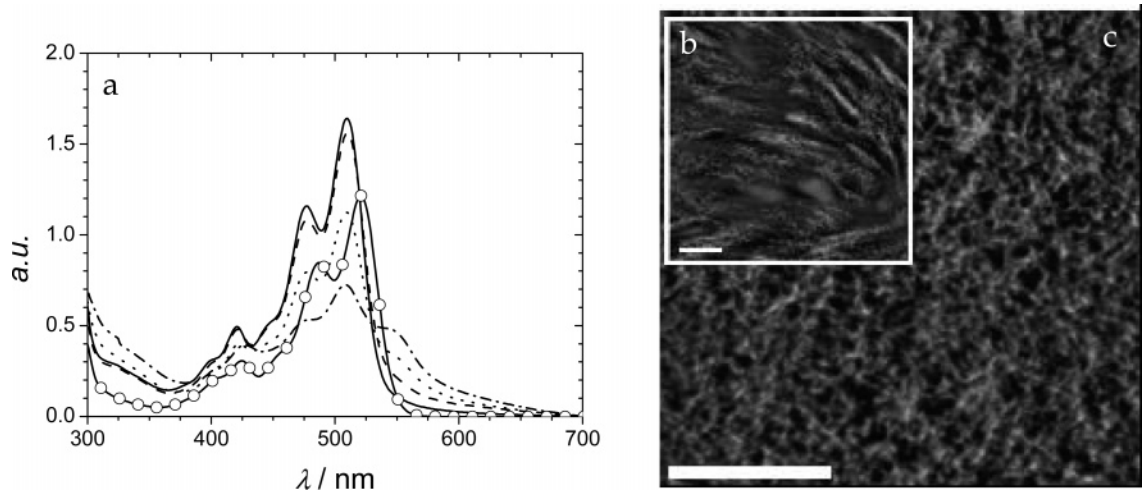

Figure 1. (a) UV/vis spectra of **PBI-1** in heptane (5×10^{-4} M, 20 °C (dash−dotted line), 40 °C (dotted line), 60 (dashed line), 80 °C (solid line)) and in dichloromethane (1.1×10^{-5} M) (20 °C, open circles). (b) and (c) TM-AFM phase images of film of **PBI-1** cast from heptane solution (z-scale 35° bars represent 250 nm).

ported.[12] In chloroform, **OPV$_4$UT** forms hydrogen-bonded dimers with a dimerization constant of $K_{dim} = 2.1 \times 10^4$ L mol^{-1} while in heptane helical stacks composed of hydrogen-bonded dimers are formed (Scheme 1).[12] The self-assembly properties of **PBI-1** (Scheme 1) were studied with temperature-dependent UV−vis measurements. The absorption spectra (Figure 1) show comparable features as found earlier for related PBs in halogenated and apolar solvents.[16,21] **PBI-1** is molecularly dissolved in dichloromethane having absorption maxima in the visible region at $\lambda_{max} = 521$, 487, and 425 nm.[21] In heptane solution, **PBI-1** is aggregated at room temperature as indicated by the red-shifted absorption maximum, $\lambda = 545$ nm. The spectrum is similar as earlier found in spin-cast films of **PB-1** indicating the formation of J-type aggregates.[16,21] At 80 °C, the shape of the absorption spectrum is comparable with that of dichloromethane solutions revealing that **PBI-1** is molecular dissolved at this temperature.

Thin Film Morphology. Thin films were fabricated by spin-coating chloroform and heptane solutions of **OPV$_4$UT** and **PBI-1** (7 g/L) onto HDMS-treated Si/SiO$_2$ substrates having source-drain gold contacts, which were employed subsequently for measuring the transport properties. These films were studied with tapping mode AFM (TM-AFM) revealing smooth films of **OPV$_4$UT** with a thickness of 75 nm and a root-mean-square (rms) roughness of 5 nm (Figure 2). For films of **OPV$_4$UT**, spun from heptane, high-resolution AFM phase images revealed individual elongated rodlike textures (Figure 2a), which are not resolved on the simultaneously recorded height image (Figure 2c). The width of the rods is constant (about 5 nm) as deduced from the line scan. Their lengths are spanning hundreds of nanometers which is in agreement with the earlier reported findings.[12] Mesoscopic domains (Figure 2b) are visible, in which columns lie straight next to each other probably as a result of side-to-side aggregation of the rods. The orientation of the domains is random, creating series of domain boundaries. In contrast, films spun from a chloroform solution (Figure 2d), completely lack the rodlike morphology. Only assemblies in the range from 5 to 50 nm in size were seen. Since **OPV$_4$UT** is molecularly dissolved in chloroform, the solid state morphology originates probably from ill-defined aggregates that are formed during the spin-coating process.[22]

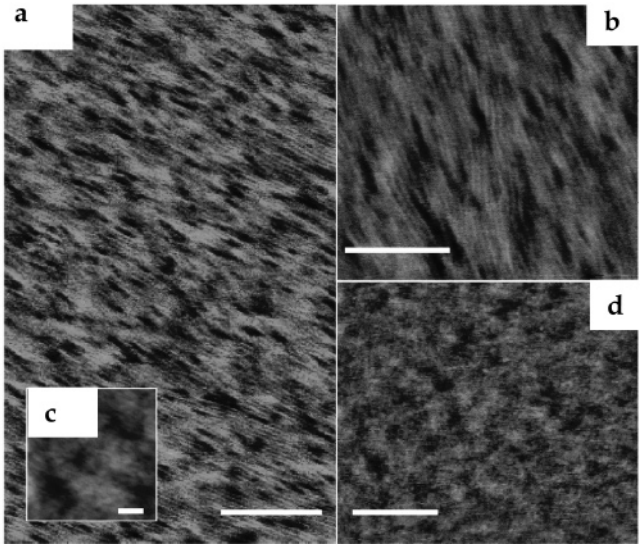

Figure 2. (a) TM-AFM phase image (z-scale 35°) of a film of **OPV$_4$UT** spun from heptane with the simultaneously recorded topography (z-scale 15 nm) in (c) and a recorded close-up phase image (z-scale 35°) *in* (b). (d) TM-AFM phase image (z-scale 5°) of a film spun from chloroform. All bars represent 100 nm.

Similar AFM results were obtained on thin films of **PBI-1**. Only when spun from heptane, the **PBI-1** films with a thickness of roughly 80 nm show a rodlike morphology (Figure 1b,c). Bundles longer than 500 nm and a diameter of 80−100 nm are observed. The smallest rods have a width of 4−5 nm and are approximately 50 nm long. On the basis of AFM data, we can conclude that the rigid columnar stacks present in heptane solutions of **OPV$_4$UT** and **PBI-1**, are transferred to a FET substrate by spin-coating.

Field-Effect Mobilities. To investigate the influence of morphology on the electrical transport between the rodlike (cast from heptane) and the amorphous morphology (cast from chloroform), FET characteristics of both films for both compounds were compared. Representative output ($I_{SD}-V_D$) and transfer ($I_{SD}-V_G$) curves were measured in the dark and under vacuum (10^{-4} mbar) at 40 °C (Figure 3). All transistors exhibit hole conduction in the case of **OPV$_4$UT**, evident from the negative gate voltages that turn the devices on. Typical on-to-

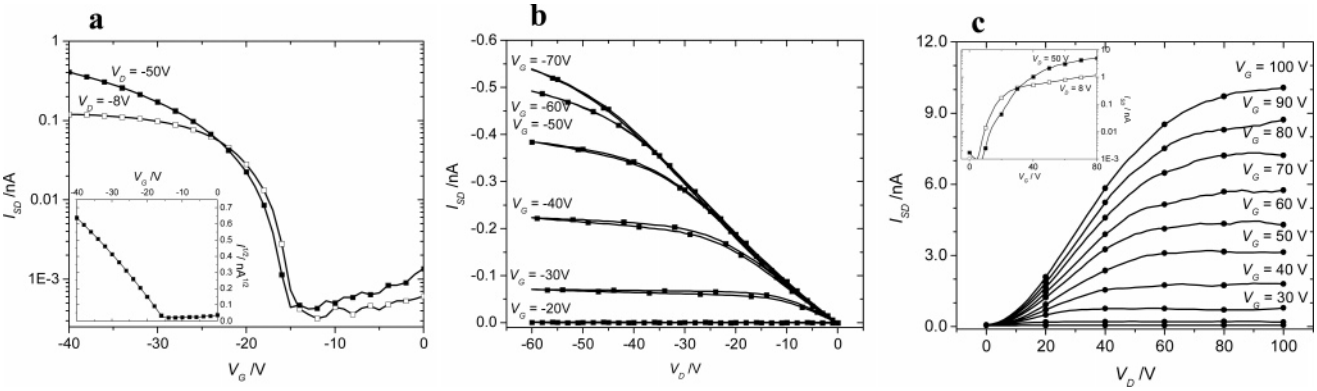

Figure 3. (a) Transfer ($I_{SD}-V_{VG}$) plotted on semilogarithmic axes for transistors of **OPV$_4$UT** spun from heptane at $V_D = -8$ V (open squares) and -50 V (solid squares). Inset shows the $I^{1/2}$ vs V_G curve for $V_D = -50$ V. (b) Output ($I_{SD} - V_D$) curves plotted for various values of V_G for **OPV$_4$UT** spun from heptane. (c) Output ($I_{SD} - V_D$) curves plotted for various values of V_G for **PBI-1** spun from heptane and inset shows the transfer ($I_{SD} - V_G$) curves at $V_D = 8$ V (open squares) and 50 V (solid squares).

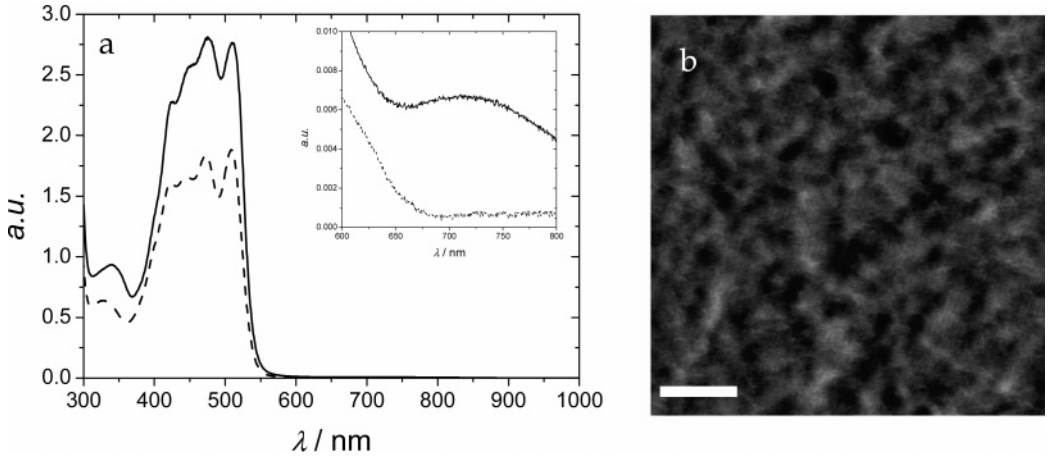

Figure 4. (a) UV−vis spectra (inset shows charge-transfer band) of a **OPV$_4$UT:PBI-1** mixture (1:1) at 20 °C (solid line) and 90 °C (dashed) line in heptane. (b) TM-AFM phase image of spin-cast **OPV$_4$UT:PBI-1** from heptane solution (z-scale 30°) (right), bar represent 100 nm.

off current ratios (I_{ON}/I_{OFF}) are $\sim 10^3-10^4$. **OPV$_4$UT** films spun from heptane show a saturated hole mobility of 1×10^{-6} cm^2/Vs deduced from the slope of the linear part of an $I_D^{1/2}$ vs V_G plot (inset Figure 3a). The output curves show indications of some contact resistance but negligible hysteresis (Figure 3b). The **OPV$_4$UT** films spun from chloroform show a mobility lower than about 10^{-7} cm^2/Vs and an I_{ON}/I_{OFF} ratio of only 10^2. The mobility measured for devices based on the solution-processed rodlike morphology is lower than earlier reported for OPVs (10^{-4} cm^2/Vs).[23] However, these values were measured either in a transistor configuration based on vacuum deposited OPV films, or in solution by the time-resolved microwave conductivity technique (measured on **OPV$_4$UT**).[13]

Films of **PBI-1** spun from heptane show electron conduction evident from the positive gate voltages that turn the transistor on (Figure 3c, I_{ON}/I_{OFF} are $\sim 10^3-10^4$) with a saturated electron mobility of 3×10^{-6} cm^2/Vs; which is about a factor of 10 000 lower than measured by time-resolved microwave conductivity.[14] The difference is due to the different frequencies used in the two different measurements. **PBI-1** devices suffers also from parasitic contact resistance effects (which are even more pronounced than in the **OPV$_4$UT** devices) originating in a strongly superlinear output characteristics at low V_D. This behavior is, however, not surprising when considering that all devices are based on Au source/drain electrodes. These electrodes are known to be nonideal for electron injection. In **OPV$_4$UT** devices, the HOMO level of **OPV$_4$UT** reasonably match the work function of Au leading to minor contact resistance problems (reasonably good hole injection, Figure 3b), whereas the mismatch between the LUMO level of **PBI-1** and Au is considerable (Figure 3c). Yet, for simplicity reason i.e., to allow straightforward comparison between devices based on **OPV$_4$UT**, PBI, and OPV−PBI mixtures, all devices were based on Au source and drain electrodes and no efforts were attempted to produce devices based on, e.g., aluminum electrodes, which certainly could improve the device performance. **PBI-1** films spun from dichloromethane did not show any reliable FET activity.

Mixed Molecular Assemblies. Self-Assembly in Solution. Mixing **OPV$_4$UT** and **PBI-1** in a 1:1 ratio in dichloromethane originates in UV−vis spectra that are summations of the spectra of the single species in this solvent; a strong indication that both compounds are molecularly dissolved and no direct interaction exist. In heptane (Figure 4) (Scheme 1), however, the characteristic red-shifted onset of aggregated **PBI-1** itself (Figure 1a) is not observed showing that the recorded spectrum is not the linear superposition of the spectra of **OPV$_4$UT** and **PBI-1** in heptane.[15] Note also that a charge-transfer band around 720 nm (ϵ = 700 L.mol^{-1}cm^{-1}) is visible, indicating the formation of an alternating OPV−PBI organization.[24] In addition, we would like to point out that the behavior of **OPV$_4$UT** and **PBI-1** in heptane is remarkably different from reported

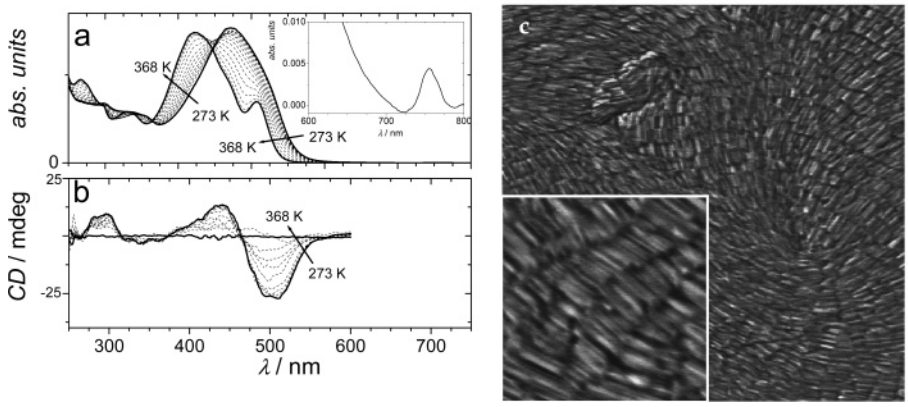

Figure 5. UV−vis (inset: show charge-transfer band) (a) and CD spectra (b) for **OPV$_4$T**:**PBI-2** (heptane, 3.1×10^{-5} M). AFM phase images of a spin-cast **OPV$_4$T**:**PBI-2** heptane solution, 10 g/L, 3.35×3.35 mm^2, z-scale 25°; inset 415×415 nm^2, z-scale 20°.

unsubstituted PBIs that show orthogonal self-assembly with **OPV$_4$UT**.[16] This dissimilarity is most probably due to the highly twisted nature[25] and the stronger electron acceptor character of the chlorinated PB derivative.[26] Indeed, it has been shown earlier that the introduction of chlorine substituents on the bay position of the PB moiety increases the tendency to form intermolecular alternating donor−acceptor complexes.[27]

To influence the supramolecular organization between OPV and PB we have investigated the coassembly between **PBI-1** and **OPV$_4$T** having additional complementary hydrogen bonding arrays. In the case of a mixture of **PBI-2** and **OPV$_4$T** (1:1) in CH_2Cl_2, the absorption and fluorescence spectra are summations of the separate components showing that they are molecularly dissolved ($\lambda_{abs}/\lambda_{em}$ in nm: **OPV$_4$T**: 426/495 and **PBI-2**: 512/540). As expected at concentrations lower than 10^{-4} M, there is no hydrogen-bonding present since the binding constant is low.[18] In heptane hydrogen-bonded **OPV$_4$T:PBI-2** complexes are present that stack through $\pi-\pi$ interactions (Scheme 1). A red-shift of the absorption maximum is found when **OPV$_4$T** is titrated with **PBI-2** and vice versa.[28] The red-shift reveals that a J-type aggregate is formed in which the **OPV$_4$T:PBI-2** complexes are cofacially oriented with an offset. This offset gives rise to a weak charge-transfer band at $\lambda_{max} = 755$ nm. A molecular absorption coefficient of $\epsilon = 130$ L·mol^{-1}cm^{-1} can be calculated based on the assumption that all molecules are participating in the aggregate. The Cotton effect of stacks of **OPV$_4$T:PBI-2** complexes as seen in the CD spectra, indicate that both chromophores are coassembled into one stack with the chirality of the OPV side chains expressed in the PBI-core.[29] Temperature dependent measurements in heptane show that the coassembly is a reversible process (Figure 5). Above 368 K, the spectral characteristics of the two components are similar to those observed in CH_2Cl_2, indicative of dissolved individual monomeric and dimeric species, whereas below 368 K, the spectra suggest that the dimers are stacked. The fluorescence quenching upon cooling to room temperature is maximal when all imide sites of **PBI-2** were hydrogen-bonded to the triazines of **OPV$_4$T**. The quenching can be explained by a photoinduced electron-transfer process between the **OPV$_4$T** donor and **PBI-2** acceptor in the stacks.[28]

Thin Film Morphology. Thin films (about 80 nm thick) were fabricated by spin-casting heptane solutions of **OPV$_4$T**:**PBI-2** (10 (1:1) g/L) and **OPV$_4$UT:PBI-1** (10 (1:1) g/L). Films of **OPV$_4$UT:PBI-1** show a structureless film morphology, possibly due to the fact that no hydrogen-boned supramolecular aggregates could form, (Figure 4b) whereas a fibrillar morphology was found for films of **OPV$_4$T**:**PBI-2** (Figure 5c). Indeed, for the latter material combination, rods of on average 110 nm are observed that associate predominantly side-by-side, evident from the lamella-width of multiples of about 3.3 nm, being the diameter of a single rod (Figure 5c, inset).[30] This dimension agrees with molecular modeling studies that estimate the length of a single **OPV$_4$T:PBI-2** as 4.1 nm (omitting dodecyloxy chains). This indicates that, in heptane, such dyads are aggregated in a J-type fashion, i.e., a tilted stack. In contrast, when **OPV$_4$T**:**PBI-2** is spin-cast from CH_2Cl_2 solutions where the two individual species are molecularly dissolved, the films showed a structureless topography.[28]

In addition, the absorption spectra of solution cast films[28] of **OPV$_4$T**:**PBI-2** from heptane and dichloromethane, respectively, are very similar to the absorption spectra in solution revealing that the supramolecular organization in solution is preserved in the solid state.

Field-Effect Mobilities. FET measurements were performed to probe the charge transport properties. Films of **OPV$_4$UT:PBI-1** from heptane lack any FET activity.[28] This behavior is surprising, as **OPV$_4$UT** and **PBI-1** on their own displayed clear FET performances with a distinct field effect (Figure 3a−c) and could be caused by unfavorable extended pathways for the opposite charges as a result of the cofacial stacking of the two chromophores. FET inactivity is unlikely due to unfavorable alignment between energy bands and/or unfavorable insulator-semiconductor interfaces, since these factors were not hampering the charge transport in the single material devices. Figure 6 shows the output and transfer characteristics of the transistor based on **OPV$_4$T:PBI-2** films having a rodlike morphology, as spun from heptane. The electronic transport shows ambipolar behavior. The transfer characteristics of the FET having the gate and drain electrodes biased negatively with respect to source

(28) See Supporting Information.
(29) Compared with stacks based on **OPV$_4$T** exclusively, the minimum is shifted from $\lambda = 427$ nm (**OPV$_4$T**) to $\lambda = 507$ nm (**OPV$_4$T**:**PBI-2**) (see Supporting Information). Jonkheijm, P.; Miura, A.; Zdanowska, M.; Hoeben, F. J. M.; De Feyter, S.; Schenning, A. P. H. J.; De Schryver, F. C.; Meijer, E. W. *Angew. Chem. Int. Ed.* **2004**, *43*, 74−78.
(30) Depositing a 3.1×10^{-5} M **OPV$_4$T**:**PBI-2** in heptane on graphite gave rods of 105 nm in length and 3.3 nm in diameter. Depositing a 4×10^{-4} M gave an interconnected network (see Supporting Information).

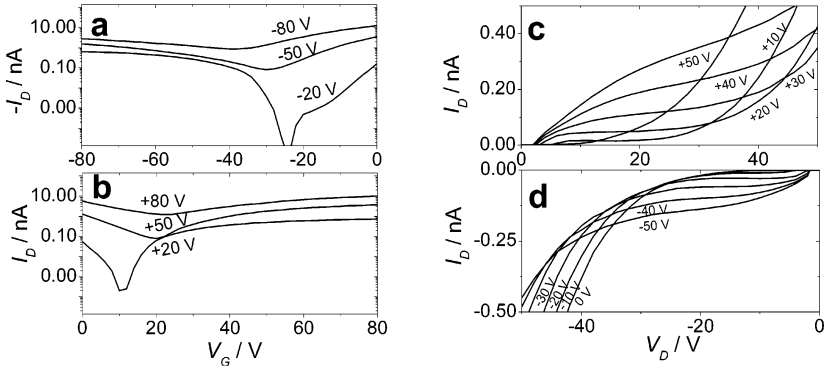

Figure 6. Transfer ($I_D - V_G$) curves at various V_D (a, b) and output ($I_D - V_D$) curves at various V_G (c, d) of FETs of **OPV$_4$T:PBI-2** cast from heptane. Hole-enhancement mode in a and d. Electron-enhancement in b and c.

electrode (Figure 6a), show that for high negative V_G the transistor operates in hole-enhancement mode. The saturated hole mobility is lower (about 2×10^{-7} cm^2/Vs), than described for **OPV$_4$UT** transistors. Note that the output curves in the p-channel mode (Figure 6d) reveal an increase in I_D for $V_D < -30$ V at $V_G = -10\ V - -30$ V. To investigate this behavior further, we measured the transfer characteristics of a film of **OPV$_4$T:PBI-2** in the electron-enhancement mode (Figure 6b). The gate and drain electrode are biased positively with respect to the grounded source electrode leading to transfer curves typical for an electron-enhancement current. The electron mobility of about 1.5×10^{-7} cm^2/Vs is lower than for the **PBI-1** devices. The electron-enhancement is clearly observed in the output curves for $V_G > 30$ V (Figure 6c). Note that in all of our measurements, the drain currents are more than a factor of 10 higher than the corresponding gate currents, emphasizing the real n-channel operation of the films.[28] The devices could be cycled more then 20 times in air and light without significant degradation while annealing to 100 °C did not change the electrical characteristics.

Our results, therefore, unambiguously illustrates that our supramolecular assembly of hole and electron conducting entities can successfully be employed to fabricate two independent pathways for the respective charge carriers. This is confirmed by the measurements on the **OPV$_4$T:PBI-2** films spun from CH_2Cl_2, which do not show any ambipolar charge transport[28] as in these films probably no interpenetrating network of donors and acceptors is created.

Conclusions

We have shown that directed supramolecular self-assembly of different entities prior to processing can be used to create a network for the two charge carriers in thin films. We have probed the ambipolar charge transport in field-effect transistors. Generic use of hydrogen-bonding interactions will allow synthetic chemists to modify the design of any building blocks of interest to incorporate them into supramolecular structures in solution that can be processes easily into thin films having a controlled functional morphology.

Acknowledgment. We thank CW−NWO and BIOMACH (P.J.), SFO (IHP; HPMI−CT-2001-00146; BBW Nr. 02.0428) (N.S.), VIDI (A.P.H.J.S.), and DFG (Wu317/5).

Supporting Information Available: Experimental conditions. This material is free of charge via the Internet at http://pubs.acs.org.

JA061966Z